Improved cross validation of a static ubiquitin structure derived from high precision residual dipolar couplings measured in a drug-based liquid crystalline phase

Alexander S. Maltsev,[a] Alexander Grishaev,[a] Julien Roche,[a] Michael Zasloff,[b] and Ad Bax[a]

[a] Laboratory of Chemical Physics, National Institute of Diabetes and Digestive and Kidney Diseases, National Institutes of Health, Bethesda, Maryland 20892-0520

[b] Georgetown University Hospital, 3800 Reservoir Rd NW, Washington, DC 20007

SUPPORTING INFORMATION

Text

Structure calculation. Structural models for ubiquitin were obtained using the Xplor-NIH program package[1] via a Cartesian molecular dynamics simulated annealing refinement protocol starting from the coordinates of the individual models corresponding to the PDB entry 1D3Z. The protocol included 100,000 steps of 1 fs each, with the temperature linearly ramped down from 2000 to 1 K and all atomic masses set to 100 a.m.u., followed by 1000 steps of Powell energy minimization. Fitted experimental restraints included all those used for obtaining the 1D3Z structure, $^{3h}J_{N\text{-}C'}$ couplings from Nisius and Grzesiek[25], as well as the newly measured $^{1}D_{NH}$, $^{1}D_{C'N}$, $^{1}D_{C'C\alpha}$ and $^{1}D_{C\alpha H\alpha}$ RDCs from the squalamine medium and $^{1}D_{HN}$, $^{1}D_{C\alpha H\alpha}$ measured in Pf1. Empirical force fields included quadratic bond, angle, and improper terms with force constants of 1000 kcal/Å^2/mol, 500 kcal/rad^2/mol and 500 kcal/rad^2/mol, respectively, as well as a quartic repulsive-only non-bonded potential with a force constant of 4 kcal/Å^2/mol and an atomic radii multiplier of 0.85. In addition, backbone/backbone hydrogen bonding geometries were restrained via a database-derived potential of mean force (H-bond PMF), described previously,[2] with the force constant multipliers of 0.3 and 0.1 for the directional and linearity terms, respectively. All RDCs were fitted with floating alignment tensors determined by SVD fits for each medium, updated every 100 simulation steps. Following the procedure used in the refinement of the 1D3Z structure, force constants for different types of RDCs were inversely proportional to the squares of the corresponding static dipolar coupling values and force constants for different media were also scaled inversely proportional to the squares of the SVD-fitted D_a values for the corresponding $^{1}D_{NH}$ couplings. The $^{1}D_{NH}$ RDC force constant multipliers (and thereby the multipliers for all remaining types of RDCs) were ramped up with a constant multiplicative factor throughout the protocol from 0.01 kcal/Hz^2/mol to 1.0 kcal/Hz^2/mol. The following force constants were used for the remaining experimental restraints: 25 kcal/ Å^2/mol for NOE distance restraints and 10 kcal/rad^2/mol for the ϕ and χ_1 dihedral angle restraints. NOE distance restraints were fitted using the soft square well potential with the "sum" option and dihedral angle restraints via a quadratic potential with no flat bottom. Structural statistics for the refined family of models are listed in the Table S7. Structures calculated with H-bond PMF and 3hJNC coupling restraint terms turned off exhibit validation statistics that are worse by 1-3% than the corresponding numbers from the structures calculated with these terms turned on (See Table S11).

Optimization of the weights for the X-ray ensemble. Values for fitting of the NMR observables to the ensemble of 15 X-ray structures, reported in Table 1 of the main text, were derived using equal weights for each of the 15 structures. This rather arbitrary choice is likely to be suboptimal, and we therefore also evaluated whether better validation statistics could be obtained by adjusting the weight factor of each of these structures. Weights for each member of the 15-chain X-ray ensemble were optimized by minimizing the rmsd between the predicted and fitted RDCs, using all available RDCs in the 4 alignment media (except for $^{1}D_{C\alpha C\beta}$ in Pf1), with the magnitude of each type of RDC in this optimization procedure scaled inversely by its static dipolar coupling value and all media scaled to have the same alignment tensor magnitudes. The calculations were done using two kinds of procedures, first as a Monte Carlo simulated annealing (with 14 adjustable weights for a 15-member ensemble and 20 parameters describing the 4 alignment tensors) followed by a Powell minimization; and second, as a successive sequence of the SVD fit of the 4 alignment tensors starting from an equally weighted ensemble, followed by the SVD fit of the 14 adjustable ensemble weights with the alignment tensors fixed and their values determined in the previous step, with the two SVD fits run iteratively till convergence of the weights was reached. When using the sequence of two SVD fits, the weight of one of the ensemble members (2D3G:A) became negative and the corresponding member was removed. The two methods of best-fitting the ensemble member weights gave virtually identical results, reported in Table S9. Optimized weights exhibit elevated, approximately equal weights for two members (1UBQ and 2ZNV:E). However, an equally weighted 2-member ensemble consisting of only these two structures exhibits worse validation statistics than the original equally weighted 15-member ensemble (data not shown). The set of optimized weights for the 15-member ensemble was then used to re-evaluate the validation statistics reported in Table 1, main text. The reweighted ensemble exhibits improved agreement with the measured $^{13}C'$ RCSA and $^{1}D_{C\alpha C\beta}$ values, while exhibiting slightly lower agreement with the measured $^{3}J_{HNH\alpha}$ values (see Table S10). The program, VW-fit, for variable weight ensemble fitting can be downloaded from http://spin.niddk.nih.gov/bax/software/

Characterization of squalamine liquid crystalline phase. The squalamine used was pharmaceutical grade (98% pure) and synthesized as the dilactate salt by Genaera Inc. (Southampton, PA) using the synthetic route described in the work by Zhang et al.[3] At neutral

pH, squalamine carries one negative and three positive charges, for a total charge of +2. It has been reported that squalamine is soluble in water up to 20 mg/ml but insoluble in 10 mM phosphate buffer.[4] Our own observations showed that squalamine is indeed poorly soluble in phosphate buffer and also at NaCl concentrations higher than ~100 mM. On the other hand we found squalamine highly soluble in imidazole buffer, and therefore this buffer (20 mM imidazole, pH 6) was used in the present work. Nevertheless, NMR spectra recorded at increasing concentrations of squalamine in imidazole buffer clearly demonstrated that it is prone to self association, in spite of its high positive charge.

Upon addition of 15 mM sodium phosphate and 5 mM hexanol, we found that a mixture of 12 mg/ml squalamine (~19 mM) yielded a birefringent suspension that strongly aligned in the magnetic field of an NMR magnet, resulting in a 10 Hz ^{2}H quadrupole splitting for the lock signal. The lyotropic liquid crystalline phase was stable over the temperature range from 1 °C to 45 °C (Figure S1) and over a wide range of concentrations, from as low as 3 mg/ml to as high as 35 mg/ml. As observed for most other liquid crystalline media used for protein NMR, the ^{2}H splitting was approximately proportional to the nematogen concentration, but decreased at higher temperatures (Figure S1).

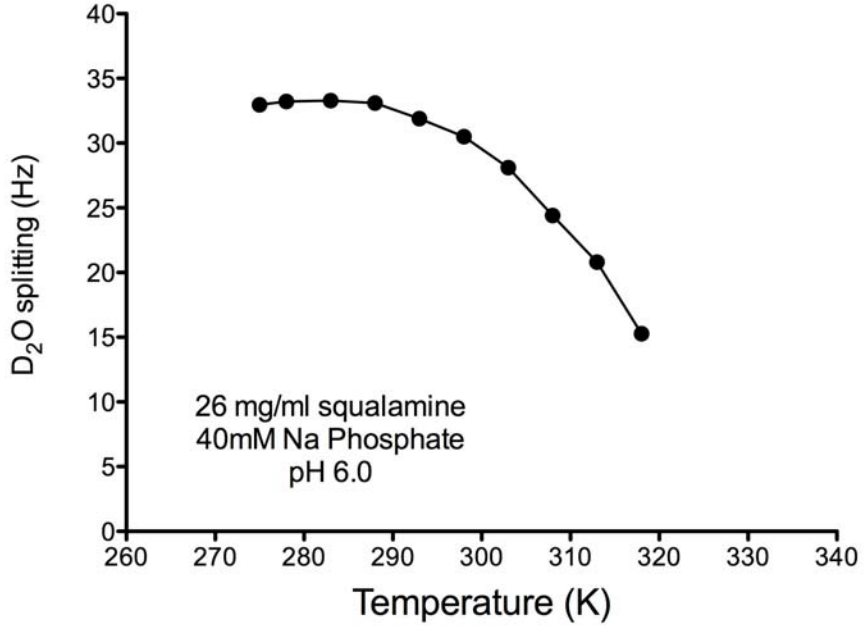

Figure S1. Temperature dependence of the D_2O splitting measured for a liquid crystalline suspension of squalamine. The sample contained 26 mg/ml of squalamine in 20 mM imidazole, pH 6.0, 40 mM sodium phosphate, 11 mM hexanol and 7 % D_2O. Spectra were recorded on a 11.7 Tesla Bruker Avance-500 system, and the sample was equilibrated for ≥20 minutes prior to each measurement. The variation in the D_2O splitting was fully reversible over the 275-308 K range.

The minimum concentration at which squalamine adopts a liquid crystalline phase was found to be quite sensitive to ionic strength. As illustrated in Figure S2, a 25 mg/mL suspension is stable up to NaCl concentrations of more than 100 mM, but at 12 mg/ml the liquid crystalline phase collapses when the ionic strength is increased above *ca* 40 mg/mL, depending on nematogen concentration.

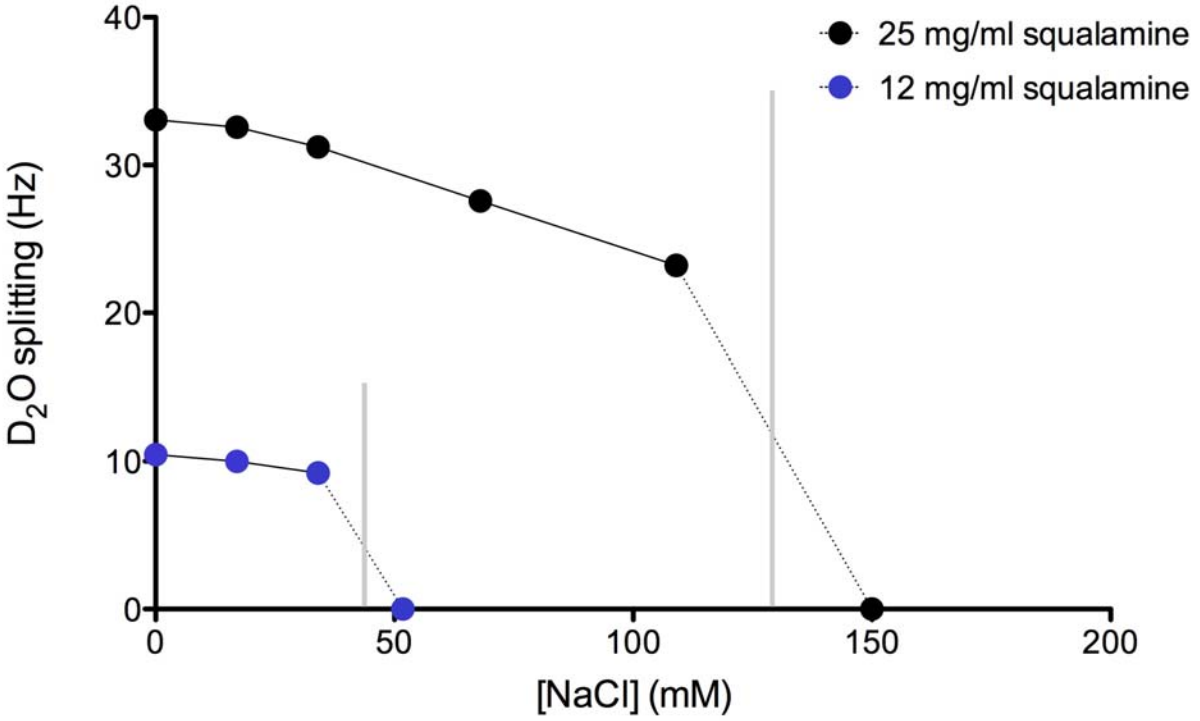

Figure S2. D_2O quadrupole splitting as a function of salt concentration, measured for a liquid crystalline suspension of squalamine. The sample with 25 mg/ml of squalamine (black dots) contains 35 mM sodium phosphate and 10 mM hexanol, while the 12 mg/ml squalamine sample (blue dots) contains 17 mM sodium phosphate and 5 mM hexanol. Both samples were prepared in 20 mM imidazole buffer, pH 6.0. Measurements were performed at 288 K, on a 11.7 Tesla Bruker Avance-500 spectrometer.

Measurement of ubiquitin RDCs. For measurements of RDCs in uniformly $^{2}H/^{13}C/^{15}N$-enriched ubiquitin (0.5 mM) in squalamine, we chose to use a low ionic strength buffer (20 mM imidazole) to create protein alignment dominated by electrostatic interaction. Alignment of ubiquitin was found to be quite strong, necessitating the use of a very dilute (3 mg/mL) but highly stable squalamine suspension (4.8 mM squalamine, 1.5 mM hexanol, 10 mM sodium phosphate, 20 mM d_4-imidazole, pH 6, 35 °C), which brought $^{1}D_{NH}$ RDCs into the ±30 Hz range, optimal for accurate measurement of RDCs in perdeuterated proteins.

$^{1}D_{NH}$ RDCs were derived from the difference in $^{1}J_{NH}+^{1}D_{NH}$ splitting measured for an isotropic sample and the aligned sample, containing 0.5 mM $\{^{2}H/^{13}C/^{15}N\}$-ubiquitin at 500 MHz ^{1}H frequency, using a 2D IPAP–HSQC experiment.[5] The IPAP-HSQC spectra were collected using

interleaved 2×180*×832* data matrices for both isotropic and aligned samples, with acquisition times of 100 ms (t_1) and 100 ms (t_2). Spectra were collected using 4 and 24 scans per FID for the isotropic and aligned sample, respectively. Spectra were processed using NMRPipe software,[6] zero-filled to yield a digital resolution of 1.7 Hz (F_1) and 2.0 Hz (F_2), and peak-picked using Sparky software.[7]

$^1D_{NC'}$ and $^2D_{HNC'}$ RDCs were derived from the difference in $^1J_{NC'}+^1D_{NC'}$ and $^2J_{HNC}+^2D_{HNC'}$ splitting, respectively, measured in the ^{15}N and ^1H dimensions of a 2D TROSY-HSQC spectrum recorded in the absence of $^{13}C'$ decoupling.[8] The TROSY-HSQC spectra were collected at 500 MHz ^1H frequency, using 240*×1049* data matrices for both isotropic and aligned samples, with acquisition times of 140 ms (t_1) and 150 ms (t_2). Spectra were collected using 4 and 32 scans per FID for the isotropic and aligned sample, respectively. Spectra were processed using NMRPipe software, zero-filled to yield a digital resolution of 0.8 Hz (F_1) and 1.7 Hz (F_2) and peak-picked using Sparky software. Resonances showed evidence of residual unresolved and in some cases resolved ^1H-^1H RDCs in the ^1H dimension, adversely affecting the precision at which $^2J_{HNC}+^2D_{HNC'}$ splittings could be measured. Therefore, $^2D_{HNC'}$ RDCs were not used for any of the structure calculations or analysis, but values are included for completeness in Tables S1 and S2.

$^1D_{C\alpha C'}$ RDCs were derived from the difference in $^1J_{C\alpha C'} + ^1D_{C\alpha C'}$ splitting, measured in the $^{13}C'$ dimension of a 3D TROSY-HNCO spectrum recorded at 600 MHz ^1H frequency in the absence of $^{13}C^{\alpha}$ decoupling during $^{13}C'$ evolution. The TROSY-HNCO spectra were collected using 2 scans per FID and 110*×80*×1024* data matrices for both isotropic and aligned samples, with acquisition times of 97 ms (t_1, $^{13}C'$), 39 ms (t_2, ^{15}N) and 136 ms (t_3, ^1H). Spectra were processed using NMRPipe software, zero-filled to yield a digital resolution of 2.2 Hz (F_1), 4.0 Hz (F_2), and 1.8 Hz (F_3), and peak-picked using Sparky software.

$^{13}C^{\alpha}$-$^1H^{\alpha}$ RDCs in Pf1 medium (13 mg/mL; 140 mM NaCl; 0.6 mM U($^{15}N/^{13}C$)-enriched ubiquitin ubiquitin, pH 6.0, 25 ºC, 600 MHz ^1H frequency) were collected using homonuclear ^1H-^1H decoupled 3D HN(CO)CA recorded in the absence of ^1H decoupling during $^{13}C^{\alpha}$ evolution , as described previously.[9] ^1H-^{15}N RDCs were collected using the ARTSY method,[10] on a sample of U($^{15}N/^{13}C/^2H$)-enriched ubiquitin ((14 mg/mL; 150 mM NaCl; 0.8 mM U($^{15}N/^{13}C$)-enriched ubiquitin, pH 6.0, 25 ºC, 800 MHz ^1H frequency), and $^{13}C^{\alpha}$-$^{13}C^{\beta}$ RDCs

were collected on the same sample, using a 3D HN(CO)CA experiment with a long (83 ms) $^{13}C^{\alpha}$ evolution time. Newly measured RDCs are included in Table S2.

Measurement of $^{1}D_{NH}$ RDCs for the ecto domain of gp41. In order to demonstrate suitability of the squalamine liquid crystal for other proteins, we carried out measurements for a loop deletion mutant of the homo-trimeric ecto domain of HIV1 coat protein gp41. The homo-trimeric arrangement is sensitive to solvent conditions, but high quality $^{1}D_{NH}$ RDCs could be measured in stretched polyacrylamide gel, and showed good agreement with the 2.4-Å X-ray structure (PDB entry 1SZT)[11] (Fig. S3A). Inducing sufficient alignment for RDC measurement in the squalamine liquid crystal required much higher concentrations than for ubiquitin (30 mg/ml) but despite the lipophilic nature of the ecto domain, virtually unchanged peak positions in the ^{1}H-^{15}N TROSY-HSQC spectrum showed no signs of direct interaction between the liquid crystal and the ecto-domain. Owing to the three-fold symmetry axis of the homotrimer, the alignment tensor is axially symmetric, and therefore (with the exception of a scaling factor) identical to that measured in the acrylamide gel. As a result, the experimental $^{1}D_{NH}$ RDCs closely correlate with one another (Figure S3B). The much smaller root-mean-square difference (rmsd) between the RDCs measured in gel and in squalamine, versus the rmsd between experimental RDCs and those fitted to the X-ray structure, indicates that the scatter in the fit of Figure S3A is dominated by uncertainty in the atomic coordinates of the X-ray structure ("structural noise")[12] and not by errors in the RDC measurements.

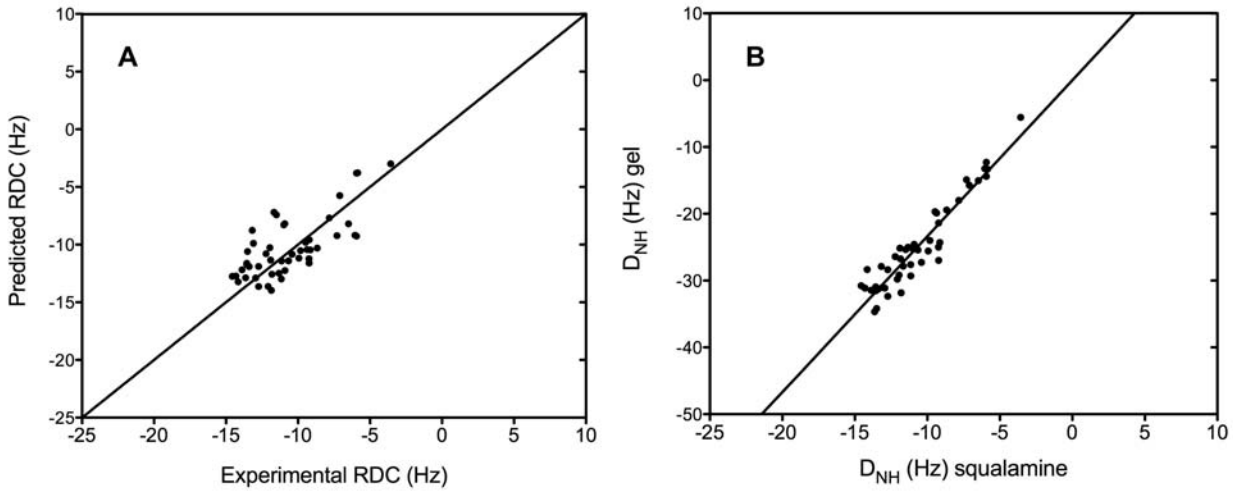

Figure S3. (A) Comparison between the $^{1}D_{NH}$ couplings measured in 30 mg/ml squalamine liquid crystal (D_a = -6.96 Hz) and the predicted $^{1}D_{NH}$ couplings based on the reference crystal structure of the g41 ectodomain (pdb entry 1SZT)[11]. RDC measurements were carried out at 300 K on a triply labeled $^{2}H/^{15}N/^{13}C$ protein sample at 0.2 mM monomer concentration, in 50 mM sodium acetate at pH 4.0, with 45 mM sodium phosphate and 13 mM hexanol. The RMSD between the experimental and the predicted $^{1}D_{NH}$ couplings is 1.97 Hz. (B) Comparison between the $^{1}D_{NH}$ couplings measured in 30 mg/ml squalamine liquid crystal and in a 4.5 % neutral stretched acrylamide gel[13,14] (radially compressed from a 6.0 mm diameter into a 4.1 mm ID NMR tube)[15]. A triply labeled $^{2}H/^{15}N/^{13}C$ protein sample at 0.25 mM monomer concentration in 50 mM sodium acetate at pH 4.0 was used for the stretched gel medium. The strength of the alignment is 2.42 times stronger in the stretched gel compared to the squalamine liquid crystal. The pairwise RMSD between the two sets of $^{1}D_{NH}$ couplings is 0.96 Hz (after scaling the stretched gel couplings by a factor of 1/2.42).

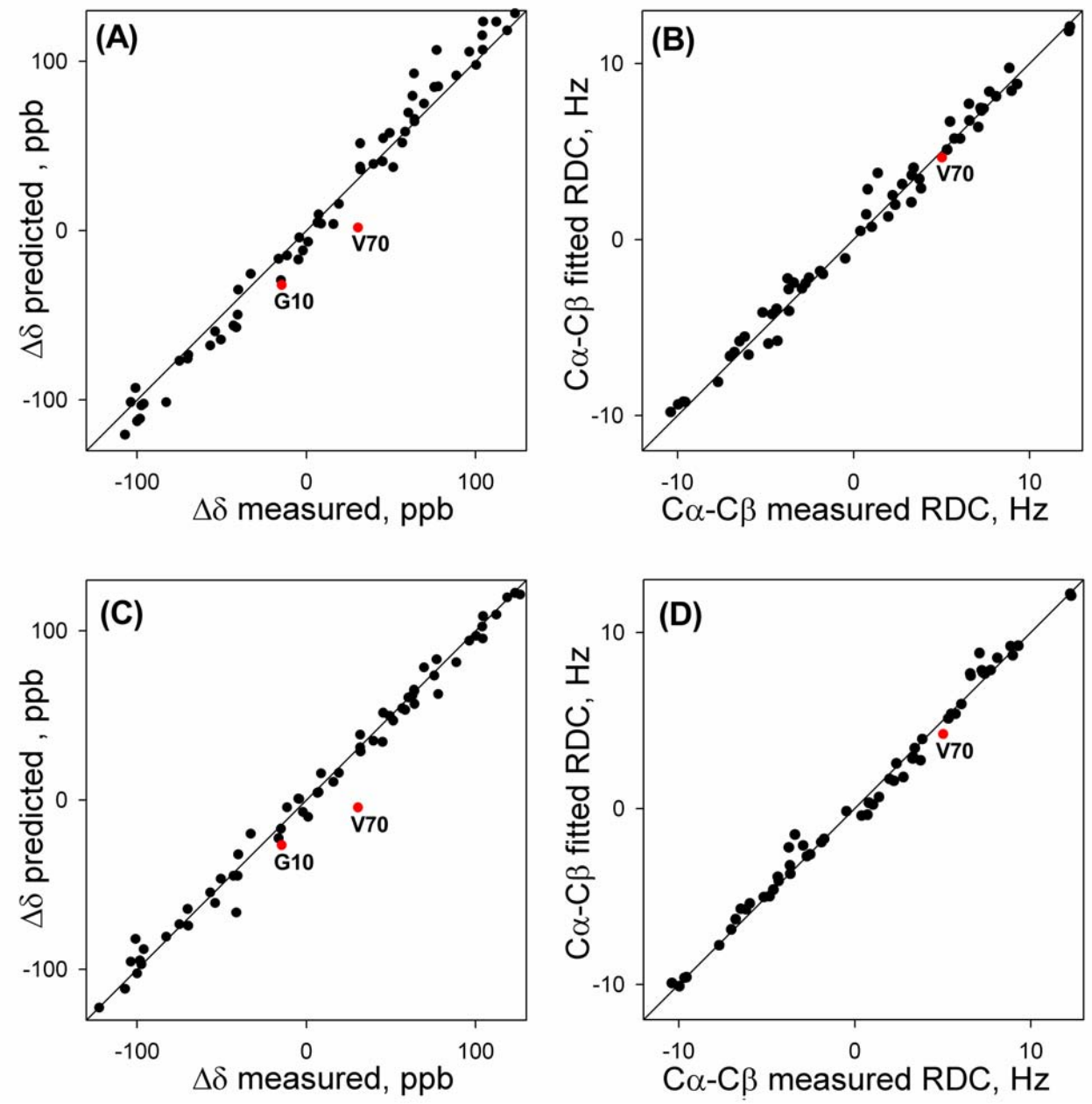

Figure S4. Correlation plots between the measured and predicted 13C' RCSA values (panels A and C) and $^{13}C^{\alpha}$-$^{13}C^{\beta}$ RDCs (panels B and D) for 2KOX (panels A and B) and X-ray (panels C and D) ensembles. The values for residues G10 and V70 are marked in red.

Table S1. Isotropic J couplings (J_{NH}, $J_{NC'}$, $J_{HC'}$, and $J_{HC'}$) measured for ubiquitin at 35 °C, 11.7 Tesla, and isotropic $^{1}J_{C\alpha C\beta}$, couplings measured at 25 °C, 14.1 Tesla, in 20 mM d_4-imidazole, pH 6.

Residue	J_{NH}, Hz (±0.02 Hz)	$J_{NC'}$, Hz (±0.02 Hz)	$J_{HC'}$, Hz (±0.03 Hz)	$J_{C\alpha C'}$, Hz (±0.03 Hz)	$J_{C\alpha C\beta}$, Hz (±0.03 Hz)	$J_{HNH\alpha}$ Hz (±0.25 Hz)
M1	—	—	—	51.45	32.39	—
Q2	-93.01	-16.57	4.84	52.96	34.55	8.19
I3	-92.91	-14.84	3.95	51.21	34.10	8.69
F4	-93.42	-16.11	4.86	52.94	32.99	9.85
V5	-92.91	-14.11	4.31	52.95	35.29	9.71
K6	-93.31	-14.38	4.40	52.74	34.78	8.71
T7	-94.28	-14.72	3.99	51.81	37.83	8.79
L8	-92.50	-14.03	4.42	52.77	33.39	3.88
T9	-92.71	-15.21	4.33	52.84	38.99	8.74
G10	-92.86	-16.21	4.59	52.58	—	—
K11	-93.37	-16.61	4.29	51.85	33.94	6.86
T12	-92.66	-15.03	4.66	52.10	37.80	9.54
I13	-92.96	-14.86	3.96	52.23	34.30	9.97
T14	-92.96	-14.90	4.28	52.21	37.55	9.26
L15	-93.82	-15.16	4.02	52.61	34.03	9.80
E16	-92.10	-14.62	4.43	52.54	35.91	9.88
V17	-93.57	-14.90	4.15	52.13	32.93	9.96
E18	-92.20	-15.61	4.17	—	—	10.08
P19	—	—	—	54.93	31.57	—
S20	-92.15	-15.90	4.62	52.20	37.71	—
D21	-94.02	-16.06	3.80	52.80	36.06	4.99
T22	-93.57	-15.41	4.25	51.51	36.97	7.66
I23	-94.02	-14.13	3.60	—	—	3.55
E24	-92.76	—	—	52.80	33.18	—
N25	-94.28	-14.93	4.32	52.69	35.45	5.10
V26	-93.62	-15.19	3.52	52.87	33.06	5.24
K27	-93.67	-14.56	4.15	52.28	33.30	3.98
A28	-94.02	-14.93	4.41	52.57	33.18	4.14
K29	-93.72	-14.99	4.03	52.34	33.33	5.05
I30	-93.77	-15.02	4.13	52.93	32.90	5.38
Q31	-93.92	-14.86	4.51	52.31	33.21	3.49
D32	-93.97	-14.98	3.65	53.15	34.43	3.18
K33	-92.81	-15.11	3.42	53.59	32.99	7.00
E34	-90.68	-14.60	3.39	53.66	34.50	8.81
G35	-94.18	-14.80	4.39	52.46	—	—
I36	-91.19	-16.21	3.36	—	—	7.05
P38	—	—	—	55.54	31.39	—
D39	-93.57	-15.10	4.18	53.07	34.94	4.67

Table S1 (continued)

Residue	J_{NH}, Hz (±0.01 Hz)	$J_{NC'}$, Hz (±0.01 Hz)	$J_{HC'}$, Hz (±0.02 Hz)	$J_{C\alpha C'}$, Hz (±0.03 Hz)	$J_{C\alpha C\beta}$, Hz (±0.01Hz)	$J_{HNH\alpha}$ Hz (±0.25 Hz)
Q40	-92.25	-15.77	4.18	52.31	35.86	8.93
Q41	-93.31	-15.93	4.49	53.43	34.33	7.57
R42	-93.42	-14.88	5.09	52.74	35.45	9.57
L43	-92.96	-14.68	4.62	53.22	34.86	9.17
I44	-92.45	-14.59	3.85	53.27	33.77	10.03
F45	-93.57	-14.20	4.34	53.21	34.56	8.28
A46	-93.92	-14.74	4.46	52.53	39.00	6.42
G47	-93.52	-15.26	3.52	52.86	—	—
K48	-93.06	-16.79	4.14	52.88	33.76	8.92
Q49	-93.16	-14.26	4.08	52.08	35.26	6.42
L50	-94.02	-14.89	3.89	53.06	34.56	6.93
E51	-92.50	-14.96	4.27	53.41	33.61	8.01
D52	-92.45	-13.74	3.90	—	—	3.41
G53	-92.30	14.39	4.18	52.41	—	—
R54	-92.81	-17.04	3.43	51.74	34.08	9.32
T55	-92.71	-15.28	3.93	52.04	37.04	9.64
L56	-94.28	-13.68	4.10	53.38	33.16	2.95
S57	-93.92	-14.90	3.80	52.06	36.59	—
D58	-94.12	-15.10	4.26	52.67	35.34	3.85
Y59	-92.35	-15.75	4.30	51.46	35.31	8.83
N60	-94.33	-15.75	4.47	52.79	41.28	7.04
I61	-93.11	-16.35	4.45	53.82	35.51	6.90
E62	-92.86	-14.78	4.63	51.70	34.14	8.91
K63	-93.37	-15.22	4.43	52.32	33.24	1.80
E64	-93.47	-15.03	4.87	52.60	37.79	6.99
S65	-93.97	-16.42	3.60	50.97	34.31	5.54
T66	-91.95	-15.12	4.30	52.32	37.53	9.89
L67	-93.01	-14.78	3.80	51.70	34.53	9.75
H68	-93.11	-14.58	4.59	52.91	34.28	9.09
L69	-93.06	-14.95	4.37	52.75	34.98	8.60
V70	-93.52	-14.87	4.37	52.10	34.10	9.50
L71	-93.01	-14.69	4.28	52.41	33.87	7.34
R72	-93.11	-14.29	3.72	52.38	34.97	7.00
L73	-93.01	-14.54	4.45	52.32	34.04	6.45
R74	-92.96	-14.64	4.07	52.67	34.69	5.91
G75	-94.12	-15.33	4.48	52.19	—	—
G76	-93.47	-17.02	3.77	—	—	—

Table S2. Ubiquitin RDCs measured in squalamine and Pf1 liquid crystalline media.

Residue	D_{NH}, Hz [a] (±0.05 Hz)	$D_{NC'}$, Hz [a] (±0.15 Hz)	$D_{HC'}$, Hz [a] (±0.2 Hz)	$D_{C\alpha C'}$, Hz [a] (±0.2 Hz)	$D_{C\alpha Ha}$, Hz [e] (±1.0 Hz)	D_{NH}, Hz [b] (±0.5 Hz)	$D_{C\alpha C\beta}$, Hz [b] (±0.15 Hz)	$D_{C\alpha H\alpha}$, Hz [c,d] (±1.5 Hz)
M1	—	—	—	-3.43	-36.9	—	0.22	-57.67
Q2	8.37	-3.52	5.15	1.61	18.8	11.82	-9.96	18.88
I3	-6.12	2.94	-2.96	-3.05	19.6	-23.11	-9.66	28.07
F4	3.07	-2.98	5.63	-3.51	5.1	-14.19	1.04	43.94
V5	9.89	2.41	-2.81	0.69	-23.6	1.41	2.37	1.66
K6	17.28	-2.32	0.09	-3.59	-34.3	27.39	7.39	-37.90
T7	15.15	2.47	-4.49	4.90	-10.9	38.14	2.76	—
L8	-17.23	2.39	-2.43	-1.12	1.4	6.89	—	—
T9	-26.58	0.23	3.67	-2.45	30.3	-27.82	3.84	—
G10	4.98	2.14	-3.59	1.03	—	37.49	—	—
K11	14.71	-2.88	2.21	-2.63	-16.4	24.27	3.41	-75.04
T12	13.01	2.07	-4.16	5.30	—	40.19	-2.93	—
I13	13.01	-1.29	-2.96	-4.01	-36.0	8.73	-4.62	-42.72
T14	11.26	0.11	0.22	6.44	-5.7	5.00	-6.48	34.72
L15	-10.89	2.10	-2.52	-3.55	1.4	-34.45	-6.77	36.40
E16	1.48	-3.91	7.56	-0.59	22.1	-7.88	7.27	15.40
V17	-9.68	1.89	-1.15	-4.11	37.0	1.91	7.72	34.12
E18	13.12	-0.24	-0.18	—	—	20.91	—	—
P19	—	—	—	-0.32	—	—	-1.90	—
S20	10.34	-4.35	3.37	-3.84	-23.5	-11.63	7.22	12.23
D21	-8.20	0.90	1.04	-1.54	—	28.00	-9.56	71.11
T22	-25.92	1.13	1.25	0.41	-10.8	-55.69	-4.32	25.21
I23	17.44	-0.71	-0.60	—	—	29.70	—	—
E24	15.53	-2.01	—	-2.41	-7.9	—	-4.84	14.50
N25	18.81	2.48	-4.82	2.40	10.6	22.99	0.39	38.50
V26	18.05	-3.59	1.47	-3.58	-29.9	22.41	8.10	-14.16
K27	15.20	2.41	-3.65	2.01	56.3	43.03	—	-4.98
A28	19.25	—	—	-2.91	—	—	3.29	-25.66
K29	15.09	1.27	-2.53	1.87	24.2	15.77	-1.74	88.17
I30	17.55	-0.97	-1.14	-2.46	-17.5	39.08	—	-67.65
Q31	13.39	-1.13	—	-1.58	11.1	37.75	-7.02	29.89
D32	19.08	1.36	-3.65	1.47	6.2	28.10	1.97	22.80
K33	16.35	-3.17	2.07	-1.32	-8.2	18.95	1.38	31.25
E34	15.09	1.69	-3.39	-2.83	-27.5	42.28	8.85	-95.27
G35	4.37	-3.33	5.60	-2.60	—	-12.04	—	—
I36	17.39	-0.09	-1.36	—	—	15.81	—	—
P38	—	—	—	-1.57	20.9	—	3.30	-29.45
D39	-16.24	1.68	0.31	5.56	-46.9	-39.28	-2.53	-46.96

Table S2 (continued)

Residue	D_{NH}, Hz (±0.05 Hz)	$D_{NC'}$, Hz (±0.15 Hz)	$D_{HC'}$, Hz (±0.20 Hz)	$D_{C\alpha C'}$, Hz (±0.20 Hz)	$D_{C\alpha Ha}$, Hz [e] (±1.0 Hz)	D_{NH}, Hz[b] (±0.50 Hz)	$D_{C\alpha C\beta}$, Hz[b] (±0.15 Hz)	$D_{C\alpha H\alpha}$, Hz[b] (±1.5 Hz)
Q40	-1.59	1.30	—	0.41	-17.8	-34.96	-6.19	14.65
Q41	-30.95	1.86	1.50	-2.30	37.3	-24.88	6.05	-29.15
R42	-2.24	-4.26	7.40	-2.29	—	—	9.29	-35.78
L43	-5.25	2.43	-1.12	0.74	-7.7	42.48	8.98	—
I44	15.80	-2.73	2.15	-3.55	-31.0	48.10	6.59	-96.63
F45	16.14	2.41	-4.34	2.13	-18.5	42.54	6.55	—
A46	15.91	-2.87	1.03	-3.26	44.5	46.42	-3.75	-35.74
G47	15.37	2.70	-4.02	2.36	—	27.90	—	—
K48	18.71	-2.75	1.36	2.52	-28.3	10.68	-3.40	20.98
Q49	11.37	1.46	-4.58	3.57	-30.3	-1.34	-3.68	-81.22
L50	14.66	-0.40	-2.89	3.28	-33.0	45.68	-2.72	-30.95
E51	18.71	-0.22	-4.27	4.04	—	8.70	-7.70	-18.88
D52	17.66	-0.19	-4.40	—	—	-2.64	—	—
G53	—	2.04	—	-3.39	—	—	—	—
R54	5.03	-3.72	6.56	-3.45	-3.4	8.32	12.29	-41.82
T55	16.51	2.52	-4.43	6.19	-25.7	18.25	3.74	—
L56	-18.26	2.24	-2.10	-2.95	—	-50.87	-5.16	—
S57	-27.23	0.21	6.19	-1.86	—	-39.19	5.72	—
D58	-10.94	1.48	0.24	6.53	-44.6	-28.59	-4.37	—
Y59	-5.30	1.32	—	-0.81	-12.8	-34.58	-3.66	18.27
N60	-30.24	1.27	3.02	-2.46	23.4	—	7.09	63.77
I61	-24.94	-0.26	4.04	-3.07	—	6.26	-0.47	65.07
E62	-27.01	-0.86	6.86	-3.23	53.2	-45.87	2.22	49.97
K63	14.21	1.85	-4.43	5.03	16.1	7.33	0.72	25.09
E64	-25.10	2.43	-1.87	0.06	-31.7	-43.39	-5.96	-12.55
S65	-31.11	1.08	2.89	-4.57	—	-22.58	-10.39	69.60
T66	-11.71	-1.19	6.19	-3.58	—	-34.26	0.80	57.07
L67	3.45	-1.42	2.70	-2.76	-10.0	-16.66	5.48	22.65
H68	16.46	1.87	-4.09	1.49	-36.6	42.05	12.24	-81.69
L69	5.52	2.80	-5.37	-1.15	-1.25	51.08	5.31	-75.35
V70	-9.14	1.91	-0.87	2.41	—	24.24	5.02	-67.50
L71	-24.83	2.83	-0.13	-3.57	50.0	-3.73	-4.77	44.24
R72	-19.41	-0.84	8.77	-1.25	35.3	-45.16	-3.01	55.72
L73	-9.79	0.26	1.04	-0.01	8.3	-21.15	0.50	36.09
R74	-2.13	-0.14	0.93	-0.70	9.1	-11.94	3.23	—
G75	-1.26	0.25	2.51	0.48	-72.6	-5.45	—	—
G76	0.22	0.37	-0.27	—	—	-2.13	—	—

[a] At 35 °C in 3 mg/ml squalamine (D_{NH}, $D_{NC'}$, $D_{HC'}$ and $D_{C\alpha C'}$) in U($^{15}N/^{13}C/^{2}H$)-enriched ubiquitin. Squalamine to hexanol molar ratio of 3.2:1; 10 mM sodium phosphate, 20 mM d_4-imidazole, pH 6. Estimated uncertainties in the reported couplings are based on line width and signal to noise [16] and do not include potentially unknown systematic errors. Reported values of the couplings involving ^{15}N incorporate the negative sign of its gyromagnetic ratio.

[b] At 25 °C in 14 mg/ml Pf1 in U($^{15}N/^{13}C/^{2}H$)-enriched ubiquitin)

[c] At 25 °C in 13 mg/ml Pf1 in U($^{15}N/^{13}C$)-enriched ubiquitin).

[d] When used for the structure refinement and X-ray ensemble weight optimization, the $^{1}D_{C\alpha H\alpha}$ RDC values were scaled up by a factor of 1.126 with respect to the values shown in Table S2 to account for the difference in alignment strengths of the U($^{15}N/^{13}C/^{2}H$)- and U($^{15}N/^{13}C$)-enriched samples.

[e] At 25 °C in squalamine using U($^{15}N/^{13}C$)-enriched ubiquitin.

Table S3. Comparison of squalamine-induced ubiquitin alignment with alignments previously reported under a variety of conditions.[a]

Alignment	Da, Hz	S_{zz}, 10^{-4}	S_{yy}-S_{xx}, 10^{-4}	S_{xy}, 10^{-4}	S_{xz}, 10^{-4}	S_{yz}, 10^{-4}	Normalized scalar product
Squalamine	-18.9	8.52	-3.77	11.50	4.82	-4.20	—
A1	3.8	-1.80	1.65	-1.77	-1.13	1.63	0.942
A2	7.7	-3.81	3.31	-3.27	-2.66	3.59	0.919
A3	18.8	-9.47	-12.60	-11.00	0.98	-0.28	0.736
A4	10.8	6.42	-4.80	4.23	-1.93	-5.17	-0.761
A5	-18.6	3.19	19.40	11.70	-0.11	-3.49	0.626
A6	-15.3	2.55	17.00	9.35	-0.33	-2.41	0.586
A7	14.1	8.53	-5.63	2.91	1.48	-8.07	-0.751
A8	5.1	3.75	0.62	1.35	1.89	-2.11	-0.827
A9	21.8	13.30	-2.40	-1.12	8.70	-9.99	-0.590
A10	8.8	5.30	-1.52	0.11	1.23	-5.23	-0.597
A11	16.8	9.84	-2.39	0.05	2.58	-10.20	-0.586
A12	15.3	9.87	-2.85	2.09	2.21	-8.69	-0.712
A13	18.1	11.90	-6.51	5.07	2.87	-9.71	-0.820
A14	12.7	8.71	0.07	4.39	1.08	-7.03	-0.823
A15	-5.9	1.81	-2.35	3.76	0.92	-2.26	0.954
A16	4.9	3.02	-1.68	1.77	-0.71	-2.42	-0.765
A17	5.9	-2.66	-2.07	-3.98	0.25	-0.62	0.788
A18	-8.8	1.60	9.88	5.05	-0.24	-2.00	0.583
A19	9.4	5.62	-0.87	-0.34	1.42	-5.63	-0.549
A20	15.3	10.10	-5.04	4.78	2.18	-8.20	-0.835
A21	4.7	-1.99	-1.74	-3.23	0.17	-0.49	0.785
A22	3.8	-1.60	-1.45	-2.60	0.19	-0.45	0.770
A23	3.2	-1.33	-1.32	-2.13	0.18	-0.40	0.753
A24	2.7	-1.16	-1.19	-1.81	0.14	-0.33	0.755
A25	3.2	-1.56	-1.90	-1.93	0.21	-0.29	0.721
A26	3.5	-1.48	-1.36	-2.42	0.13	-0.39	0.779
A27	-8.8	3.05	-2.37	5.70	1.40	-3.09	0.973
A28	-3.1	0.55	2.20	2.36	-0.06	-0.01	0.703
A29	7.9	4.82	-3.02	3.30	-1.69	-3.53	-0.760

Table S3 (continued)

Alignment	Da, Hz	S_{zz}, 10^{-4}	S_{yy}-S_{xx}, 10^{-4}	S_{xy}, 10^{-4}	S_{xz}, 10^{-4}	S_{yz}, 10^{-4}	Normalized scalar product
A30	-13.9	4.62	10.80	8.66	0.12	-2.99	0.764
A31	-20.4	5.90	17.50	13.00	-0.07	-2.65	0.715
A32	-12.4	4.52	9.23	7.30	-0.07	-3.39	0.771
A33	-9.6	3.95	7.16	5.34	0.06	-2.68	0.775
A34	-9.9	3.93	6.12	5.88	0.70	-2.72	0.841
A35	6.5	4.41	0.91	2.07	0.31	-3.65	-0.784
A36	-3.1	0.57	2.23	2.39	-0.05	-0.03	0.708

[a] Alignment conditions A1-A36 follow the notation of Lange et al.,[17] summarized in Table S4. For each alignment condition the components of the Saupe matrix were calculated by SVD-fitting the reported $^{1}D_{NH}$ RDCs to the NMR-based static structure 1D3Z (model A). Saupe matrices were used to calculate the normalized scalar products between each alignment condition and the squalamine alignment, following the procedure of Sass et al.[18]

Table S4. Summary of alignment conditions A1-A36 used by Lange et al.[17]

A#	Description of the alignment medium	Reported in
A1	7% positively charged gel, APTMAC:acrylamide = 1:3, 50 mM NaP	Lakomek[19]
A2	7% positively charged gel, APTMAC:acrylamide = 1:1, 50 mM NaP	Lakomek[19]
A3	5% negatively charged gel, acrylic acid: acrylamide = 1:1, 50 mM NaP	Lakomek[19]
A4	5% PEG(C12E5):hexanol, 50 mM NaP	Lakomek[19]
A5	25 mg/ml Pf-1 phage, 50 mM NaP, 100 mM NaCl	Lakomek[19]
A6	20 mg/ml Pf-1 phage, 50 mM NaP, 100 mM NaCl	Lakomek[19]
A7	15% neutral bicelles, DMPC:DHPC = 3:1, 50 mM NaP, 50 mM NaCl	Lakomek[19]
A8	5% negative bicelles, DMPC:DHPC:SDS = 30:10:2, 50 mM NaP	Lakomek[19]
A9	10% negative bicelles, DLPC:DHPC:SDS = 30:10:2, 50 mM NaP	Lakomek[19]
A10	5% neutral bicelles, DMPC:DHPC:C14PC = 30:10:1, 50 mM NaP	Lakomek[19]
A11	10% neutral bicelles, DMPC:DHPC:C14PC = 30:10:2, 50 mM NaP	Lakomek[19]
A12	10% positive bicelles, DMPC:CHAPSO:CTAB = 50:10:1, 50 mM NaP	Lakomek[19]
A13	8% positive bicelles, DMPC:CHAPSO:CTAB = 30:10:1, 50 mM NaP	Lakomek[19]
A14	7% neutral gel, 50 mM NaP	Lakomek[20]
A15	3.5% cetylpyridinium bromide : hexanol = 1:1, 50 mM NaP, 25 mM NaBr	Lakomek[20]
A16	5% PEG(C12E5):hexanol, 50 mM NaP	Lakomek[20]
A17	4 mg/ml purple membrane, 50 mM NaP, 50 mM NaCl	Lakomek[20]
A18	15 mg/ml Pf-1 phage, 50 mM NaP, 400 mM NaCl	Lakomek[20]
A19	5% neutral bicelles, DMPC:DHPC = 3:1, 10 mM NaP, pH 6.6	Ottiger[21]
A20	5% posititve bicelles, DMPC:DHPC:CTAB = 30:10:1, 10 mM NaP, pH 6.6	Ottiger[21]

Table S4 (continued)

A#	Description of the alignment medium	Reported in
A21	2 mg/ml purple membrane, 20 mM NaCl, pH 7.2	Briggman[22]
A22	2 mg/ml purple membrane, 40 mM NaCl, pH 7.2	Briggman[22]
A23	2 mg/ml purple membrane, 60 mM NaCl, pH 7.2	Briggman[22]
A24	2 mg/ml purple membrane, 80 mM NaCl, pH 7.2	Briggman[22]
A25	8 mg/ml purple membrane, 250 mM NaCl, pH 7.2	Briggman[22]
A26	1.5 mg/ml purple membrane, 20 mM NaCl, pH 7.2	Briggman[22]
A27	3.4% cetylpyridinium bromide : hexanol = 1:1.33, 75 mM NaBr, pH 6.6	Briggman[22]
A28	3.5 mg/ml Pf-1, 20 mM NaCl, pH 6.6	Briggman[22]
A29	4.2% PEG(C12E5):hexanol, pH 6.6	Briggman[22]
A30	4 mg/ml Pf-1, 5% acrylamide, 10 mM Mg^{2+}, polymerized at 55° angle	Ruan[23]
A31	4 mg/ml Pf-1, 5% acrylamide, 10 mM Mg^{2+}, polymerized at 0° angle	Ruan[23]
A32	3 mg/ml Pf-1, 5% acrylamide, 10 mM Mg^{2+}, polymerized at 30° angle	Ruan[23]
A33	3 mg/ml Pf-1, 5% acrylamide, 20 mM Mg^{2+}, polymerized at 30° angle	Ruan[23]
A34	3 mg/ml Pf-1, 5% acrylamide, 10 mM Mg^{2+}, polymerized at 55° angle	Ruan[23]
A35	5% neutral gel, pH 6.6	Ruan[23]
A36	3.5 mg/ml Pf-1 phage, pH 6.6	Ruan[23]

Table S5. Structural validation statistics for all available ubiquitin X-ray structures solved at a resolution ≤1.8 Å. All predicted data are calculated separately over each individual chain and averaged between the chains in cases where multiple chains are present for a given deposition.

PDB ID	Chain ID	Resolution (A)	^{13}C' RCSA rmsd [e] (ppb)	Q_{NH} [d,e,f] (%)	$Q_{C\alpha C\beta}$ Pf1 [d] (%)	$^{3}J_{HNH\alpha}$ rmsd [e] (Hz)
1P3Q[a,b]	U,V	1.70	12.72/13.00	19.9/18.5	20.8	0.872/0.852
1UBI	A	1.80	13.29/13.13	19.3/17.8	20.4	0.897/0.829
1UBQ	A	1.80	14.57/14.33	17.7/17.0	20.7	0.838/0.771
1WRD[a,b]	B	1.75	14.20/14.25	28.8/27.5	21.6	1.385/1.264
2D3G [a,b]	A,B	1.70	14.97/14.90	21.5/20.0	16.0	0.880/0.805
2ZCC [a]	A,B,C	1.40	14.28/14.12	21.8/20.3	19.9	0.827/0.804
2ZNV [a,b]	B,C,E	1.60	8.65/8.97	20.7/17.2	14.1	0.903/0.811
3BY4 [a,b]	B	1.55	14.24/13.82	24.3/22.4	18.4	0.976/0.909
3ONS [a]	A	1.80	12.59/12.76	21.6/20.9	18.5	1.119/1.080
<X-ray> [c]	All	All	8.32/8.14	14.6/12.2	10.4	0.661/0.567

[a] Data collected at cryogenic temperature

[b] Ubiquitin as part of the complex with another protein

[c] When calculating the predicted values over the entire ensemble in the same manner as reported in the Table 1, main text.

[d] All Q factors are reported using D_a and R values obtained from the SVD fit to the entire X-ray ensemble.

[e] ^{13}C' Validation statistics are given both for the case where the H^N has been modeled on the line bisecting the C'-N and N-C^{α} bonds (first number), and after adding the same out of plane angle to the N-H vector that is observed in the newly derived NMR structure (second number).

[f] Average Q-factor for the four sets of $^{1}D_{NH}$ RDCs used in the present study.

Table S6. Above the diagonal: Root-mean-square deviation between the predicted ^{13}C' RCSA values in ppb (averaged over multiple chains when present) for the available ubiquitin X-ray structures solved at a resolution ≤1.8 Å. Below the diagonal: Pairwise backbone coordinate rmsd (N, C^{α}, C') over residues 2-70. On the diagonal: backbone coordinate rmsd to mean for X-ray structures with multiple ubiquitin chains.

PDB entry	1P3Q	1UBI	1UBQ	1WRD	2D3G	2ZCC	2ZNV	3BY4	3ONS
1P3Q	0.50	16.16	17.49	16.61	15.19	12.39	11.75	16.77	12.86
1UBI	0.524	-	5.92	12.29	13.79	16.50	14.62	14.25	13.55
1UBQ	0.532	0.080	-	14.34	14.95	17.18	16.16	16.02	14.40
1WRD	0.553	0.411	0.414	-	16.35	16.26	15.47	18.44	16.88
2D3G	0.500	0.416	0.419	0.470	0.23	15.98	12.32	11.50	11.18
2ZCC	0.496	0.530	0.535	0.589	0.679	0.23	10.18	17.18	13.42
2ZNV	0.513	0.427	0.435	0.334	0.354	0.588	0.19	12.62	11.55
3BY4	0.465	0.424	0.436	0.424	0.314	0.630	0.338	-	13.54
3ONS	0.461	0.403	0.407	0.495	0.325	0.557	0.437	0.382	-

Table S7. Structural statistics for the final refined family of 20 ubiquitin models (PDB entry 2MJB).

R.m.s. to mean (C'/Cα/N, res. 1-72)	0.07Å
R.m.s. to mean of 1D3Z (C'/Cα/N, res.1-72)	0.20±0.02 Å
R.m.s. bond violation	$(1.11\pm0.01)*10^{-2}$ Å
R.m.s. angle violation	0.94±0.01º
R.m.s. improper torsion angle violation	0.83±0.01º
Clashes/1000 atoms[a]	0.97
R.m.s. dihedral restraint violation	6.9±0.6º
R.m.s. distance restraint violation	$(2.4\pm0.1)*10^{-2}$ Å
Fitted $^{1}D_{NH}$ RDC Q-factor, neutral bicelles	0.050±0.006
Fitted $^{1}D_{NH}$ RDC Q-factor, charged bicelles	0.054±0.003
Fitted $^{1}D_{NH}$ RDC Q-factor, squalamine	0.088±0.006
Fitted $^{1}D_{NH}$ RDC Q-factor, Pf1	0.075±0.004
% Ramachandran favored (res. 1-72)[a]	100
Average database H-bond directional energy[c]	-4.9±0.5 kT
Average database H-bond linearity energy[c]	0.48±0.02 kT
R.m.s. $^{3h}J_{N-C'}$ coupling violation[b]	0.101±0.003 Hz

[a] Molprobity[24] was used for the clash and Ramachandran statistics.

[b] Experimental $^{3h}J_{N-C'}$ values were derived from the pressure- and temperature dependent data from Nisius and Grzesiek[25] as described in the paper and fitted using Eq. 12 of Barfield et al.[26]

[c] Calculated as described in reference 2.

Table S8. Experimental validation statistics for two earlier NMR ensemble representations of ubiquitin.[a]

structure	2K39[17]	1XQQ[27]
RCSA[b] (ppb)	9.0/14.5/9.9 [b]	11.5/24.0/15.6 [b]
Q_{NH}[c] (%)	6.7/9.9/7.2	20.3/50.9/28.4
$Q_{C\alpha C\beta}$ (%)	11.1/13.5/11.4	17.4/13.6/17.0
$^3J_{HNH\alpha}$ [d] (Hz)	0.67/0.80/0.69	0.98/1.66/1.13

[a] For Q2-V70. Predicted $^{13}C'$ RCSA values are based on the alignment tensor obtained from an SVD fit of the $^1D_{NH}$ RDCs, previously reported in conjunction with the RCSA values,[28] to the ensemble of models. Therefore, there are no RCSA-fitted adjustable parameters used in this comparison. [b] The first number corresponds to residues with ≤0.4 Å backbone coordinate (N, C^α, C') rmsd in the X-ray ensemble; the 2nd number to residues with >0.4 Å rmsd (7-11, 32-35, 46, 47, 52, and 70); the 3rd number to all residues. [c] Average Q-factor for the four sets of $^1D_{NH}$ RDCs used in the present study. 2K39 lacked squalamine $^1D_{NH}$ but the working RDCs spanned the entire five-dimensional alignment space. 1XQQ was derived without RDCs, and reported values therefore correspond to free Q factors.
[d] RMSD relative to $^3J_{HNH\alpha}$ predicted using "rigid" Karplus equation coefficients of Vogeli et al.[29]

Table S9. Optimized weights of the X-ray ensemble members, best-fitted via Monte Carlo simulated annealing/Powell minimization against the sets of RDCs used for calculating the static ubiquitin structure. N-H vector orientations were obtained by adding the same out of plane angle that is observed in the newly derived static NMR structure. Averages and standard deviations over 1000 independent runs are reported.

PDB ID	Chain ID	Optimized weight
1P3Q	U	$9.9\pm0.2\ 10^{-2}$
	V	$4\pm2\ 10^{-3}$
1UBI	A	$8.3\pm0.5\ 10^{-2}$
1UBQ	A	$1.79\pm0.05\ 10^{-1}$
1WRD	B	$1.3\pm0.1\ 10^{-2}$
2D3G	A	$9\pm6\ 10^{-8}$
	B	$7.2\pm0.2\ 10^{-2}$
2ZCC	A	$6.3\pm0.3\ 10^{-2}$
	B	$6.4\pm0.2\ 10^{-2}$
	C	$2.8\pm0.2\ 10^{-2}$
2ZNV	B	$4.1\pm0.2\ 10^{-2}$
	C	$5.9\pm0.2\ 10^{-2}$
	E	$2.18\pm0.01\ 10^{-1}$
3BY4	B	$2.2\pm0.1\ 10^{-2}$
3ONS	A	$5.6\pm0.2\ 10^{-2}$

Table S10. Comparison of the validation statistics for equally weighted ensemble of X-ray structures with weight factors determined by SVD-fitting the sets of RDCs used for calculating the static ubiquitin structure. $^{3}J_{HNH\alpha}$ rmsds are given both for the case where the H^N atom has been modeled on the line bisecting the C'-N and N-C^α bonds, and after adding the same out-of-plane angle to this vector that is observed in the newly derived NMR structure.

	^{13}C' RCSA (ppb)	$Q_{C\alpha C\beta}$ (%)	Q_{NH} (%) [a]	$^{3}J_{HNH\alpha}$ rmsd, Hz
Equally weighted ensemble	8.14	10.4	12.2	0.661/0.567
Reweighted ensemble with weights from Table S9	7.76	9.8	10.7	0.666/0.585

[a]Average Q-factor for the four sets of $^{1}D_{NH}$ RDCs used in the present study.

Table S11. Comparison of the newly derived NMR structures calculated with and without H-bonding PMF (HBDB) and $^{3}J_{NC}$ coupling terms.

	^{13}C' RCSA (ppb)	$Q_{C\alpha C\beta}$ (%)	$^{3h}J_{HNH\alpha}$ rmsd, Hz
With HBDB and $^{3}J_{NC}$ terms	8.85	11.7	0.50
Without HBDB and $^{3}J_{NC}$ terms	8.89	11.8	0.52

References

(1) Schwieters, C. D.; Kuszewski, J. J.; Clore, G. M. *Prog. Nucl. Magn. Reson. Spectrosc.* **2006**, *48*, 47-62.
(2) Grishaev, A.; Bax, A. *J. Am. Chem. Soc.* **2004**, *126*, 7281-7292.
(3) Zhang, X. H.; Rao, M. N.; Jones, S. R.; Shao, B.; Feibush, P.; McGuigan, M.; Tzodikov, N.; Feibush, B.; Sharkansky, I.; Snyder, B.; Mallis, L. M.; Sarkahian, A.; Wilder, S.; Turse, J. E.; Kinney, W. A.; Kjaersgaard, H. J.; Michalak, R. S. *J. Org. Chem.* **1998**, *63*, 8599-8603.
(4) Selinsky, B. S.; Zhou, Z.; Fojtik, K. G.; Jones, S. R.; Dollahon, N. R.; Shinnar, A. E. *Biochimica Et Biophysica Acta-Biomembranes* **1998**, *1370*, 218-234.
(5) Yao, L. S.; Ying, J. F.; Bax, A. *J. Biomol. NMR* **2009**, *43*, 161-170.
(6) Delaglio, F.; Grzesiek, S.; Vuister, G. W.; Zhu, G.; Pfeifer, J.; Bax, A. *J. Biomol. NMR* **1995**, *6*, 277-293.
(7) Goddard, T. D.; Kneller, D. G. University of California, San Francisco, 2008.
(8) Wang, Y. X.; Marquardt, J. L.; Wingfield, P.; Stahl, S. J.; Lee-Huang, S.; Torchia, D.; Bax, A. *J. Am. Chem. Soc.* **1998**, *120*, 7385-7386.
(9) Ying, J.; Roche, J.; Bax, A. *J. Magn. Reson.* **2014**, *in press*.
(10) Fitzkee, N. C.; Bax, A. *J. Biomol. NMR* **2010**, *48*, 65-70.
(11) Tan, K. M.; Liu, J. H.; Wang, J. H.; Shen, S.; Lu, M. *Proc. Natl. Acad. Sci. U. S. A.* **1997**, *94*, 12303-12308.
(12) Zweckstetter, M.; Bax, A. *J. Biomol. NMR* **2002**, *23*, 127-137.
(13) Tycko, R.; Blanco, F. J.; Ishii, Y. *J. Am. Chem. Soc.* **2000**, *122*, 9340-9341.
(14) Sass, H.-J.; Musco, G.; Stahl, S. J.; Wingfield, P. T.; Grzesiek, S. *J. Biomol. NMR* **2000**, *18*, 303-309.
(15) Chou, J. J.; Gaemers, S.; Howder, B.; Louis, J. M.; Bax, A. *J. Biomol. NMR* **2001**, *21*, 377-382.
(16) Kontaxis, G.; Clore, G. M.; Bax, A. *J. Magn. Reson.* **2000**, *143*, 184-196.
(17) Lange, O. F.; Lakomek, N. A.; Fares, C.; Schroder, G. F.; Walter, K. F. A.; Becker, S.; Meiler, J.; Grubmuller, H.; Griesinger, C.; de Groot, B. L. *Science* **2008**, *320*, 1471-1475.
(18) Sass, J.; Cordier, F.; Hoffmann, A.; Rogowski, M.; Cousin, A.; Omichinski, J. G.; Lowen, H.; Grzesiek, S. *J. Am. Chem. Soc.* **1999**, *121*, 2047-2055.
(19) Lakomek, N. A.; Walter, K. F. A.; Fares, C.; Lange, O. F.; de Groot, B. L.; Grubmuller, H.; Bruschweiler, R.; Munk, A.; Becker, S.; Meiler, J.; Griesinger, C. *J. Biomol. NMR* **2008**, *41*, 139-155.
(20) Lakomek, N. A.; Carlomagno, T.; Becker, S.; Griesinger, C.; Meiler, J. *J. Biomol. NMR* **2006**, *34*, 101-115.
(21) Ottiger, M.; Bax, A. *J. Am. Chem.Soc.* **1998**, *120*, 12334-12341.
(22) Briggman, K. B.; Tolman, J. R. *J. Am. Chem. Soc.* **2003**, *125*, 10164-10165.
(23) Ruan, K.; Tolman, J. R. *J. Am. Chem. Soc.* **2005**, *127*, 15032-15033.
(24) Chen, V. B.; Arendall, W. B., III; Headd, J. J.; Keedy, D. A.; Immormino, R. M.; Kapral, G. J.; Murray, L. W.; Richardson, J. S.; Richardson, D. C. *Acta Crystallogr. Sect. D-Biol. Crystallogr.* **2010**, *66*, 12-21.

(25) Cordier, F.; Grzesiek, S. *Journal of American Chemical Society* **1999**, *121*, 1601-1602.
(26) Barfield, M. *J. Am. Chem. Soc.* **2002**, *124*, 4158-4168.
(27) Lindorff-Larsen, K.; Best, R. B.; DePristo, M. A.; Dobson, C. M.; Vendruscolo, M. *Nature* **2005**, *433*, 128-132.
(28) Cornilescu, G.; Bax, A. *J. Am. Chem. Soc.* **2000**, *122*, 10143-10154.
(29) Vogeli, B.; Ying, J. F.; Grishaev, A.; Bax, A. *J. Am. Chem. Soc.* **2007**, *129*, 9377-9385.
(30) Cornilescu, G.; Marquardt, J. L.; Ottiger, M.; Bax, A. *J. Am. Chem. Soc.* **1998**, *120*, 6836-6837.
(31) Fenwick, R. B.; Esteban-Martin, S.; Richter, B.; Lee, D.; Walter, K. F. A.; Milovanovic, D.; Becker, S.; Lakomek, N. A.; Griesinger, C.; Salvatella, X. *J. Am. Chem. Soc.* **2011**, *133*, 10336-10339.
(32) Richter, B.; Gsponer, J.; Varnai, P.; Salvatella, X.; Vendruscolo, M. *J. Biomol. NMR* **2007**, *37*, 117-135.
(33) Vijay-Kumar, S.; Bugg, C. E.; Cook, W. J. *J. Mol. Biol.* **1987**, *194*, 531-544.